Comprehensive Speciation Analysis of Residual Gadolinium in Deep Cerebellar Nuclei in Rats Repeatedly Administered With Gadoterate Meglumine or Gadodiamide

Izabela Strzeminska, Cecile Factor, Javier Jimenez-Lamana, Sabrina
Lacomme, Maria Angels Subirana, Philippe Le Coustumer, Dirk Schaumlöffel,
Philippe Robert, Joanna Szpunar, Claire Corot, et al.

HAL Id: hal-03651800
https://univ-pau.hal.science/hal-03651800

Submitted on 26 Apr 2022

ORIGINAL ARTICLE

Comprehensive Speciation Analysis of Residual Gadolinium in Deep Cerebellar Nuclei in Rats Repeatedly Administered With Gadoterate Meglumine or Gadodiamide

Izabela Strzeminska, PhD,*† Cecile Factor, PhD,* Javier Jimenez-Lamana, PhD,† Sabrina Lacomme,‡§ Maria Angels Subirana, PhD,† Philippe Le Coustumer, PhD, Dsc,‡§ Dirk Schaumlöffel, PhD, Dsc,† Philippe Robert, PhD,* Joanna Szpunar, PhD, Dsc,† Claire Corot,* and Ryszard Lobinski, PhD, Dsc†‖

Purpose: Several preclinical studies have reported the presence of gadolinium (Gd) in different chemical forms in the brain, depending on the class (macrocyclic versus linear) of Gd-based contrast agent (GBCA) administered. The aim of this study was to identify, with a special focus on insoluble species, the speciation of Gd retained in the deep cerebellar nuclei (DCN) of rats administered repeatedly with gadoterate or gadodiamide 4 months after the last injection.

Methods: Three groups (N = 6/group) of healthy female Sprague-Dawley rats (SPF/OFA rats; Charles River, L'Arbresle, France) received a cumulated dose of 50 mmol/kg (4 daily intravenous administrations of 2.5 mmol/kg, for 5 weeks, corresponding to 80-fold the usual clinical dose if adjusted for man) of gadoterate meglumine (macrocyclic) or gadodiamide (linear) or isotonic saline for the control group (4 daily intravenous administrations of 5 mL/kg, for 5 weeks). The animals were sacrificed 4 months after the last injection. Deep cerebellar nuclei were dissected and stored at −80°C before sample preparation. To provide enough tissue for sample preparation and further analysis using multiple techniques, DCN from each group of 6 rats were pooled. Gadolinium species were extracted in 2 consecutive steps with water and urea solution. The total Gd concentrations were determined by inductively coupled plasma mass spectrometry (ICP-MS). Soluble Gd species were analyzed by size-exclusion chromatography coupled to ICP-MS. The insoluble Gd species were analyzed by single-particle (SP) ICP-MS, nanoscale secondary ion mass spectroscopy (NanoSIMS), and scanning transmission electron microscopy with energy-dispersive X-ray spectroscopy (STEM-EDX) for elemental detection.

Results: The Gd concentrations in pooled DCN from animals treated with gadoterate or gadodiamide were 0.25 and 24.3 nmol/g, respectively. For gadoterate, the highest amount of Gd was found in the water-soluble fractions. It was present exclusively as low-molecular-weight compounds, most likely as the intact GBCA form. In the case of gadodiamide, the water-soluble fraction of DCN was composed of high-molecular-weight Gd species of approximately 440 kDa and contained only a tiny amount (less than 1%) of intact gadodiamide. Furthermore, the column recovery calculated for this fraction was incomplete, which suggested presence of labile complexes of dissociated Gd^{3+} with endogenous molecules. The highest amount of Gd was detected in the insoluble residue, which was demonstrated, by SP-ICP-MS, to be a particulate form of Gd. Two imaging techniques (NanoSIMS and STEM-EDX) allowed further characterization of these insoluble Gd species. Amorphous, spheroid structures of approximately 100–200 nm of sea urchin-like shape were detected. Furthermore, Gd was consistently colocalized with calcium, oxygen, and phosphorous, strongly suggesting the presence of structures composed of mixed Gd/Ca phosphates. No or occasional colocalization with iron and sulfur was observed.

Conclusion: A dedicated analytical workflow produced original data on the speciation of Gd in DCN of rats repeatedly injected with GBCAs. The addition, in comparison with previous studies of Gd speciation in brain, of SP element detection and imaging techniques allowed a comprehensive speciation analysis approach. Whereas for gadoterate the main fraction of retained Gd was present as intact GBCA form in the soluble fractions, for linear gadodiamide, less than 10% of Gd could be solubilized and characterized using size-exclusion chromatography coupled to ICP-MS. The main Gd species detected in the soluble fractions were macromolecules of 440 kDa. One of them was speculated to be a Gd complex with iron-binding protein (ferritin). However, the major fraction of residual Gd was present as insoluble particulate species, very likely composed of mixed Gd/Ca phosphates. This comprehensive Gd speciation study provided important evidence for the dechelation of linear GBCAs and offered a deeper insight into the mechanisms of Gd deposition in the brain.

Key Words: gadolinium, GBCA, gadoterate, gadodiamide, deep cerebellar nuclei, speciation, SEC-ICP-MS, NanoSIMS, STEM-EDX

(*Invest Radiol* 2022;57: 283–292)

I n 2014, it was suggested that repeated administration of linear gadolinium-based contrast agents (GBCAs) leads, in healthy patients, to T1 signal enhancement in specific brain structures, such as globus pallidus and dentate nuclei in magnetic resonance (MR) imaging.[1,2] Also, unexpected presence of gadolinium (Gd) in other parts of the brain was demonstrated using inductively coupled plasma mass spectrometry (ICP-MS),[3,4] challenging the widely accepted assumption that GBCAs cannot cross a healthy blood-brain barrier. The Gd accumulation in brain has not been associated with any toxicological effect or disorder. However, the causal relationship of nephrogenic systemic fibrosis with several linear GBCAs (L-GBCAs) in patients with severe renal failure was evoked in 2006.[5–7] Therefore, Gd presence in brain has been attracting the attention of regulatory agencies, such as the European Medical Agency and Food and Drug Administration.[8–10]

Very quickly, a preclinical model of rat with T1 signal enhancement in the deep cerebellar nuclei (DCN) similar to human dentate nuclei was developed,[11,12] facilitating the investigation of the Gd retention mechanisms. The relationship between the chemical structure of GBCAs and the amount of total Gd accumulated in tissue was established: significantly higher concentrations were found in brain tissues

after administration of L-GBCAs in comparison with macrocyclic GBCAs (M-GBCAs), which might be related to their different stabilities.[13] Indeed, as L-GBCAs (open-chain structure) are less kinetically stable than M-GBCAs (cage-like structure),[14] it was suggested that they may partly degrade in vivo.[15] Two processes may simultaneously occur: transmetallation (Gd^{3+} exchange by endogenous cations such as Fe^{3+} or Cu^{2+}, Zn^{2+} and Ca^{2+}) and transligation (exchange of polyaminocarboxylic ligand by several anions such as PO_4^{3-}, CO_3^{2-}, OH^-, and citrate). This leads to an alteration of the initial Gd-ligand equilibrium in a GBCA complex. Interestingly, DCN, which are the major site of increased signal intensity after L-GBCA administrations, are simultaneously one of the richest in iron brain structures.[16,17] Once dissociated from GBCA, Gd^{3+} can interact with the biological environment, creating new Gd species responsible for its prolonged or permanent deposition. For instance, dissociated Gd^{3+} can bind to soluble macromolecules, which would increase significantly the relaxivity, supporting previously observed T1 signal enhancement on MR images. Another possibility is that Gd^{3+} can form insoluble precipitates such as $GdPO_4$, $Gd_2(CO_3)_3$, or $Gd(OH)_3$, which have poor relaxivity, or form "composite insoluble structures" with a potential nonnegligible contribution to the T1 signal enhancement.[18] Consequently, an exhaustive characterization of residual Gd species is essential for the understanding of the long-term GBCAs safety.[19]

Several studies addressed the retention and speciation of Gd in the central nervous system,[20] but only a few of them focused specifically on the DCN accumulating the highest amount of Gd. Indeed, recent laser ablation (LA)-ICP-MS studies[17,21] showed the long-term Gd retention occurring preferentially in DCN, with the Gd concentrations as high as 34 to 40 nmol/g (5.4–6.2 ppm) and no clear correlation between Gd and phosphorus, copper, or zinc.[17] Whereas LA-ICP-MS is an adequate technique for the determination of Gd localization in the brain, it lacks the ability to identify whether Gd is present as the chelated GBCA form or dechelated Gd^{3+} form. Therefore, this approach by itself cannot answer the questions of Gd speciation in DCN.

High-resolution transmission electron microscopy (TEM) demonstrated sea urchin–shaped Gd deposits in the basal membrane of DCN microvessels and sometimes small electron-dense dots in the pigment aggregates located in the glial cells of rats treated with L-GBCAs.[22] Apart from Gd, phosphorus and, to smaller extent, sulfur and calcium were detected by nanoscale secondary ion mass spectrometry (NanoSIMS) in these insoluble deposits. These findings are consistent with the hypothesis of Gd deposition in the form of insoluble $GdPO_4$. However, because of the sample preparation typically used with TEM and NanoSIMS, these techniques allow only for detection of insoluble Gd species and other soluble forms of Gd cannot be excluded.

Complementary speciation data can be obtained by chromatography coupled with Gd-specific or GBCA-specific detection by ICP-MS[23,24] or electrospray MS,[25] respectively. In the major brain structures such as cerebellum, cortex, or subcortical brain, it was previously shown that for L-GBCAs, at least 4 distinctive Gd species were present: small water-soluble molecules such as intact GBCAs, soluble macromolecules (with size estimations of superior to 66 kDa or of approximately 200–300 kDa), labile complexes of Gd^{3+} with endogenous biomolecules, and in majority as insoluble species that were not further characterized.[23–26] So far, speciation studies using hyphenated techniques were limited to the analysis of larger brain structures and the tiny DCN (±9 mg) have never been analyzed separately from the cerebellum. Furthermore, Gd contained in the insoluble brain fraction was not analyzed in terms of speciation because of the lack of mild solubilization methods, rendering the studies incomplete in terms of mass balance of Gd, especially for the L-GBCAs.

Therefore, the aim of this study was to analyze the speciation of the entirety of residual Gd (present 4 months post injection) in DCN of rats administered with 2 GBCAs: 1 macrocyclic and ionic (gadoterate meglumine) and 1 linear and nonionic (gadodiamide). For this reason, the DCN were carefully dissected and solubilized in 2 subsequent steps of water and urea extraction allowing for complete recovery of soluble Gd species,[26] which were further analyzed using size exclusion chromatography coupled to ICP-MS. The speciation analysis of the remaining Gd in the insoluble DCN fraction was studied using single-particle (SP) ICP-MS, NanoSIMS, and scanning TEM (STEM) with energy-dispersive X-ray spectrometry (EDX).

MATERIALS AND METHODS

All animal experiments were conducted in full compliance with the European Union Directive 2010/63/EU on the protection of animals used for scientific purposes.

Analytical reagent grade chemicals were used. They were obtained from Merck (Darmstadt, Germany) unless stated otherwise. Dionized water (18 MΩ cm) was obtained from a Milli-Q water purification system (Merck, Darmstadt, Germany).

Animal Model and GBCA Administration

Three groups (N = 6/group) of healthy female Sprague-Dawley rats (SPF/OFA rats; Charles River, L'Arbresle, France) randomly received 4 intravenous administrations per week at 1 per day for 5 weeks (20 intravenous injections in total) of 2.5 mmol/kg of either gadoterate meglumine (0.5 M; Dotarem, Guerbet, Villepinte, France) or gadodiamide (0.5 M; Omniscan, GE Healthcare, Boston, MA) or isotonic saline for the control group. All the animals received the injections on the same days of the week. Intravenous injections were performed in a tail vein under isoflurane anesthesia (IsoFlo, Axience, Pantin, France). The animals were sacrificed 4 months (M4) after the last injection. Upon completion of the wash-out period, the rats were euthanized under isoflurane anesthesia by exsanguination. The DCN were dissected. The localization of DCN in the rat brain is shown in Figure 1 in Supplemental Digital Content (SDC), http://links.lww.com/RLI/A663. DCN from 6 animals were pooled together to provide enough tissue (~50 mg) for sample preparation and further analysis. The cerebral tissues were stored at −80°C before sample preparation.

Sample Preparation

Figure 1 summarizes the sample preparation procedure. The tissue (~50 mg) was homogenized using a Bead Ruptor homogenizer (Omni International, Kennesaw, GA) in 0.5 mL of 100 mM ammonium acetate pH 7.4 (dilution factor of 11). Then, the homogenate was centrifuged using the Centrifuge system 5804 R (Eppendorf, Hamburg, Germany) for 30 minutes at 20,800g at 4°C, and the supernatant was separated from the pellet. The remaining pellet was washed with 0.5 mL of 100 mM ammonium acetate and centrifuged at 20,800g for 30 minutes at 4°C and then solubilized in 1 mL of 5.6 M urea by probe sonication. Then, the solution was centrifuged at 20,800g for 30 minutes at 4°C. The urea-soluble supernatant was collected and stored at 4°C. It was diluted with 100 mM ammonium acetate pH 7.4 (dilution factor 2) and centrifuged at 20,800g for 30 minutes at 4°C before size-exclusion chromatography (SEC) analysis. The urea-insoluble fraction was washed once with 1 mL of ultrapure water to remove the remaining urea and was stored at −20°C. The final pellet was resuspended in 0.5 mL of water and probe sonicated to obtain homogenous aqueous slurry that was further analyzed by SP-ICP-MS, NanoSIMS, and TEM.

Total Gd Determination

Samples of tissue homogenate and soluble and insoluble fractions of DCN (0.1 mL) were digested on a hot plate with a mixture (3:1, v/v) of nitric acid and hydrogen peroxide (0.4 mL) at 80°C for 8 hours, followed by dilution with water (dilution factor of 10 or 100). In this last step, indium was added as internal standard to obtain a final concentration of 1 ng/mL. The total Gd concentrations were measured with ICP-MS using a 7900 ICP-MS (Agilent Technologies, Santa Clara, CA). The ICP-MS instrument used for the total Gd determination was optimized daily using a multielemental solution. A
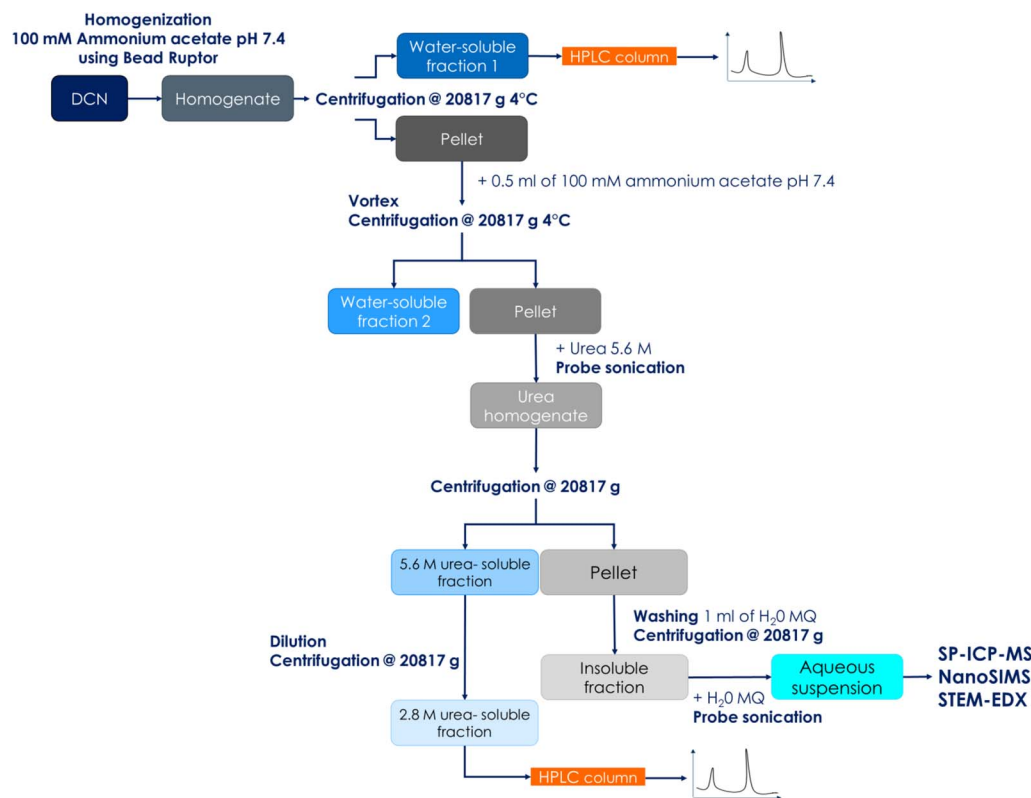
FIGURE 1. Sample preparation procedure and resulting fractions.

standard curve of inorganic Gd in 4% HNO_3 was used by monitoring the response of the ^{158}Gd isotope. The quantification range of the method was either 0.005 or 0.010 to 1.0 ng/mL in solution. The Gd concentration in each fraction of cerebral tissue (homogenate and supernatant) was expressed as nmol/g and was calculated by multiplying the Gd concentration measured in the final solution by the dilution factor applied during sample preparation, including the homogenization step for calculation for the cerebral tissue. The lower limit of quantification (LLOQ) of Gd was 0.04 nmol/g in wet tissue, complying with the criterion that the analyte response at the LLOQ should be at least 5 times the analyte response of the zero calibrator.

Extraction Efficiency Measurement

To evaluate the amount of soluble Gd extracted from the cerebral tissue to the supernatant, the extraction efficiency was calculated using the following equation:

$$\text{extraction efficiency} \left(\% \frac{\text{mol}}{\text{mol}}\right) = \frac{n_{\text{Gd supernatant}}}{n_{\text{Gd homogenate}}} \times 100, \text{ where } n_{\text{Gd}} \text{ is}$$

the number of moles of Gd.

Gd Speciation Analysis

The SEC-ICP-MS analysis was carried out using an HPLC 1260 system (Agilent) coupled to a model 7700x ICP-MS (Agilent). Gd species were isocratically eluted from a Superdex-200 column (300 × 10 mm; GE Healthcare) with 100 mM ammonium acetate (pH 7.4) over 45 minutes at a flow rate of 0.7 mL/min. The injection volume was 100 µL. The LLOQ of SEC-ICP-MS was estimated using standard GBCA solutions and set at 0.3 pmol/mL for both GBCAs. The LLOQ was determined respecting the criteria that the signal-to-noise ratio should be at least 5. To control the background level of Gd, the supernatant obtained from the sample of the control group

was analyzed at the beginning and at the end of the sequence as the blank. The average blank chromatogram per run was calculated and subtracted from the chromatograms.

SP-ICP-MS Analysis

All the aqueous slurries of the insoluble residue were diluted 1000-fold in water to ensure that only an SP will enter the ICP-MS at a time. A model 7900 ICP-MS (Agilent) with a single nanoparticle application module for ICP-MS and MassHunter software (Agilent) was used for SP analysis. ^{158}Gd was monitored with a dwell time of 100 microseconds during a total acquisition time of 60 seconds.

NanoSIMS Analysis

For gadodiamide samples, the suspension of insoluble DCN fraction was deposited on a Si wafer and air-dried overnight in a desiccator. The solid residue was coated with a 5-nm gold layer using a Cressington 108 Auto sputter-coater (Cressington, Watford, UK). Elemental distribution was analyzed by NanoSIMS, performed with a NanoSIMS 50 L (Cameca, Gennevilliers, France). A Hyperion RF plasma primary oxygen ion source (Oregon Physics, Beaverton, OR) was used for the mapping of calcium (^{40}Ca$^+$), iron (^{56}Fe$^+$), and Gd (^{155}Gd$^+$ and ^{158}Gd$^+$). A primary Cs$^+$ ion source was used for the mapping of oxygen (^{16}O$^-$), carbon (^{12}C$_2$), nitrogen (^{12}C^{14}N$^-$), sulfur (^{32}S$^-$), and phosphorus (^{31}P). Detection was achieved in parallel using electron multiplier detectors. Mass calibration was performed with standards prepared in the same manner as the sample and mass resolution was adjusted to resolve possible interferences. Cluster ions (ie, ^{12}C^{14}N$^-$) were used to maximize the signal measured for the element of interest (^{14}N). Gd-rich structures were localized by means of a preliminary screening of 28 consecutive regions of the sample and the ones containing Gd were subsequently analyzed in detail. For each region, a 60 × 60 µm area was presputtered with a 425 pA beam of O$^-$ primary ions, during

7 minutes. Afterward, images of 15 × 15 μm or 25 × 25 μm were acquired within that area, with a 5.0 pA beam, 256 × 256 pixels, a dwell time of 10 milliseconds per pixel, and a spatial resolution of approximately 100 nm.

The same areas were mapped with Cs^+ primary ions, with the same raster size, pixel, and dwell time, after presputtering with Cs^+ primary ions. A beam of 1.0 pA was applied on the sample, attaining a spatial resolution of approximately 100 nm. Image processing was performed using WinImage (Cameca). Several cycles of the same area were acquired and stacked to obtain the final image. Spatial resolution was calculated by the knife-edge method (16%–84% criterion).[27]

STEM-EDX Analysis

For gadodiamide samples, 1 droplet of the suspension of insoluble DCN fraction was deposited on a copper grid covered with a amorphous carbon thin film, and air-dried during 2h under a protective glass cup. The TEM-STEM-EDX was a Talos F200S (Thermo Fischer Scientific, Waltham, MA) working at 200 keV, equipped with a field emission gun. The emission rate was with a C2 aperture of 50 μm (nominal diameter). Bright field and high resolution up to 800 k maximum magnification were used to image the morphology, dimension, and texture of the material. Selected area diffraction was used to resolve the state of the material (amorphous or crystallized) using a microprobe of 4 upon a scale of 10, a camera length of 1 m, and a diffraction diaphragm aperture of 40 μm (nominal diameter). For STEM-EDX mode, the operational parameters were a C2 of 50 μm, a nanoprobe of 4 upon a scale of 10, an aperture with a converge angle of 7.5 mrad, and camera length of 260 mm to optimize the spatial resolution (around 0.5 nm) and X photons rate (between 800 and 1100 counts/s). The X-EDS spectra and maps were drawn using Velox software. The TEM and STEM images were converted to .tiff format after their treatment with Digital Micrograph software (Gatan, Pleasanton, CA). The spectra and elemental maps were transferred to .tiff format using Velox software (Thermo Fisher Scientific, Waltham, MA).

RESULTS

Total Gd Determination

Gd concentrations in the pooled DCN from the animals treated with a cumulative dose of 50 mmol/kg of macrocyclic gadoterate meglumine and linear gadodiamide, after a 4-month wash-out period, were 0.25 and 24.3 nmol/g, respectively. Gd concentration in the DCN of animals from the control group was less than the LLOQ of the method ($LLOQ_{tissue} = 0.04$ nmol/g). Figure 2 shows the amount of Gd extracted in each fraction obtained using the sequential extraction protocol. For gadoterate, the highest amount of Gd was measured in the water-soluble fractions (0.83 ng) and a smaller amount was found in the insoluble fraction (0.47 ng). Because of the very low quantity of residual Gd observed for gadoterate at M4, the Gd concentration after the addition of the urea solution was less than the lower limit of the quantification ($LLOQ_{5.6M\ urea} = 0.007$ nmol/g). For gadodiamide, 3.10 ng of Gd was found in water-soluble and 11.8 ng in the urea-soluble fractions. Further dilution of the urea fraction with ammonium acetate buffer (pH 7.4) decreased 4 times the amount of soluble Gd (2.76 ng). Seventy percent of total Gd was still present in the insoluble fraction (110 ng). The concentrations of total, water-soluble, urea-soluble, and insoluble Gd in ng and nmol per g of wet DCN tissue are presented in Table 1 in SDC, http://links.lww.com/RLI/A663.

The mass balance was 83% for gadoterate and 80% for gadodiamide. As the DCN samples from 6 animals were pooled, the analytical replicates were not available to improve the quality of the data and the results should be regarded as an approximation and not a determination.
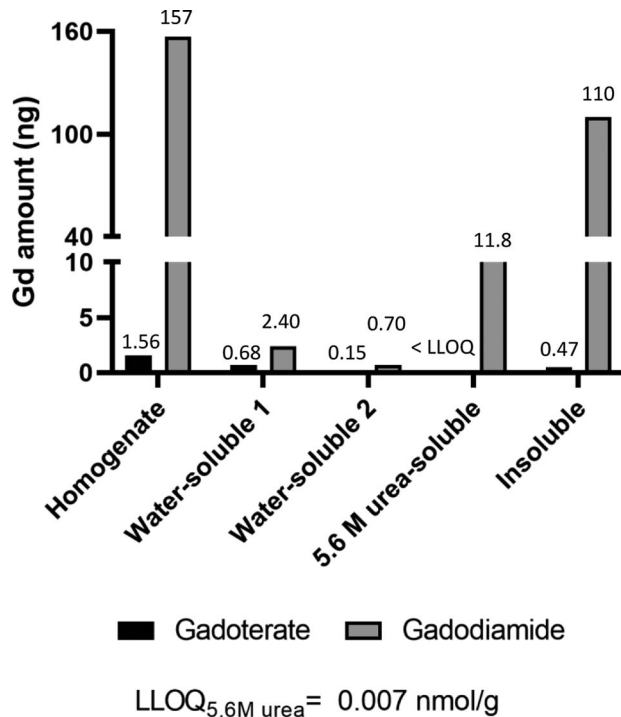

FIGURE 2. Amount of Gd in different fractions of pooled DCN after repeated injections of either gadoterate or gadodiamide using the sequential extraction protocol.

Speciation of Soluble Gd Using SEC-ICP-MS

Figure 3 shows the ^{158}Gd chromatograms obtained for water-soluble and urea-soluble fractions of DCN. Whereas for gadoterate only 1 peak eluting at 28.3 minutes was detected in the water-soluble fraction, the same elution time as that of the intact GBCA form, for gadodiamide, 2 different peaks were detected at the retention times $RT_1 = 20.2$ minutes and $RT_2 = 28.5$ minutes. The same chromatogram overlapped with the signal for ^{54}Fe (Fig. 4) showing the coelution of Gd with iron peak at 20.2 minutes. The column recoveries were 95% and 32% for gadoterate and gadodiamide, respectively, suggesting for the latter the presence of another Gd species in that fraction. The washing of the water-insoluble fraction allowed the recovery of additional portion of Gd species that were already detected in water-soluble fractions for both gadoterate and gadodiamide. This result showed that some part of Gd species was retained in the insoluble fraction by physical interactions.

Only a small peak was detected at the retention time of 28.3 minutes in the urea-soluble fraction of DCN for gadoterate. For gadodiamide, 3 Gd species were observed: 1 at $RT_1 = 11.0$ minutes and 2 at the same retention times as the Gd species in the water-soluble fraction at $RT_2 = 20.2$ minutes and $RT_3 = 28.5$ minutes.

According to column calibration (cf. Fig. 2 in SDC, http://links.lww.com/RLI/A663), Gd eluting at 11.0 minutes is bound to macromolecules with a molecular weight of more than 660 kDa, whereas Gd eluting at 20.0 minutes is bound to macromolecules with a molecular weight of approximately 440 kDa. In addition, elution times between 24.0 and 30.0 minutes correlated with molecules in the range 0.238 to 44 kDa, which matches the molecular weight of the intact GBCA forms (approximately 0.5 kDa).

Insight Into the Residual Gd Form by SP-ICP-MS

Figure 5 shows the ^{158}Gd time scans obtained using SP-ICP-MS for an ionic Gd^{3+} standard and for the insoluble residue of DCN from
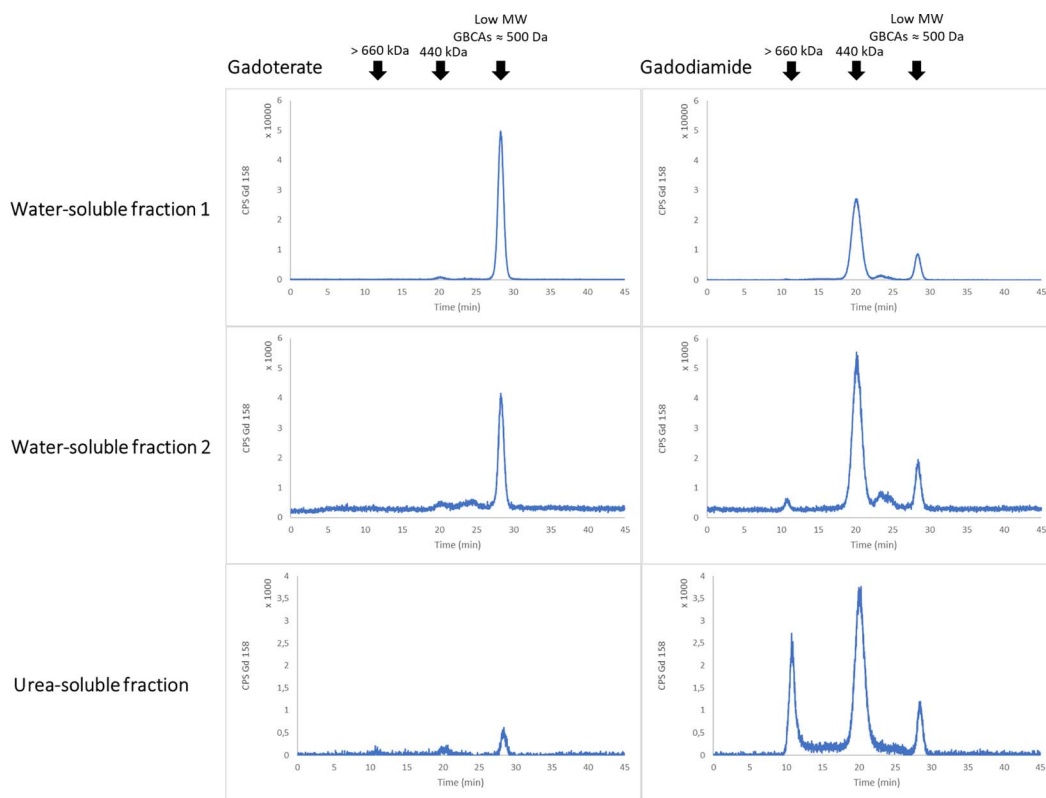
FIGURE 3. Typical SEC-ICP-MS ^{158}Gd chromatograms of the water and urea-soluble fractions of the DCN from the animals treated with gadoterate or gadodiamide. MW indicates molecular weight.

untreated animals and treated with gadoterate meglumine and gadodiamide. The time scan obtained for the gadodiamide sample presents a significant number of spikes above the background, each of them corresponding to a single-bearing Gd particle that demonstrates the presence of the particulate form of Gd in the final pellet obtained through sequential extraction procedure. In contrast to that, no Gd spikes were observed for the gadoterate and the control group samples in the analysis conditions.

NanoSIMS Characterization of the Insoluble Gd Species

From the 28 regions of 60 μm × 60 μm that were screened by NanoSIMS, 14 Gd-containing structures were detected in 7 regions. Figure 6 presents the NanoSIMS images of one of these regions obtained using oxygen and cesium as the primary ion beam. The NanoSIMS analysis revealed the presence of ellipsoid areas rich in
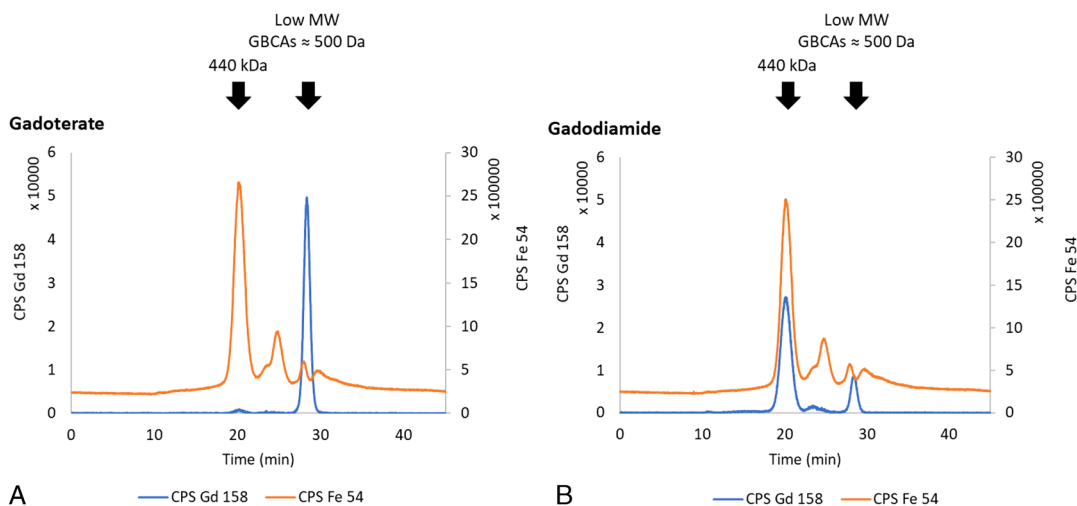

FIGURE 4. SEC-ICP-MS ^{158}Gd and ^{54}Fe chromatograms of water-soluble fraction of the DCN from the animals treated with gadoterate (A) or gadodiamide (B). MW indicates molecular weight. CPS, counts per second.
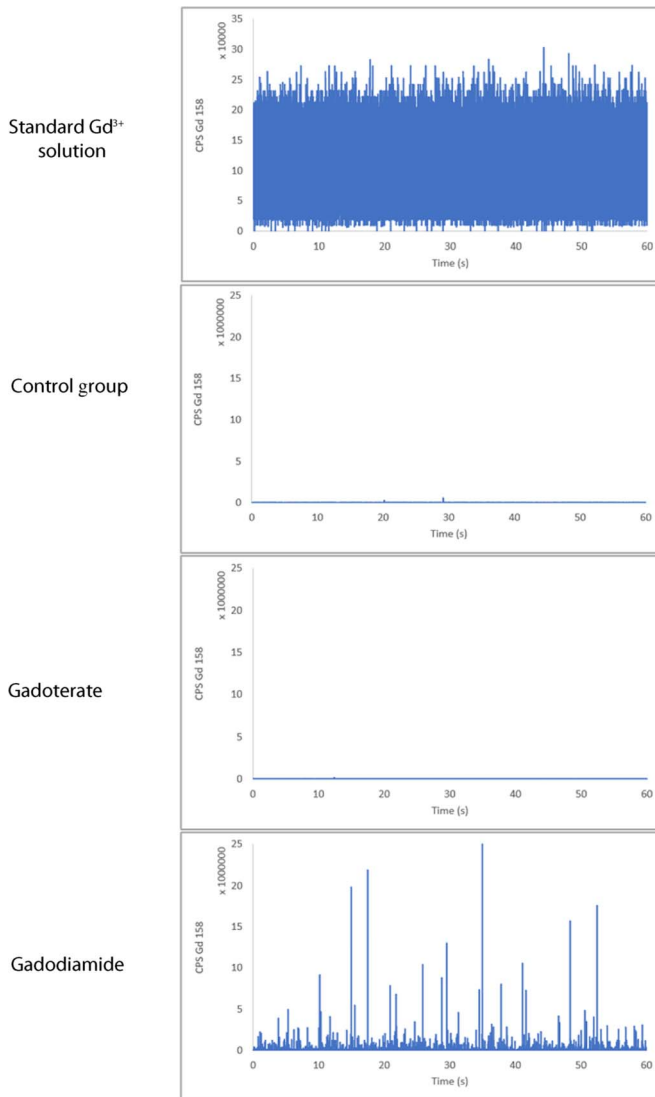
FIGURE 5. SP-ICP-MS ^{158}Gd time scans obtained for ionic Gd^{3+} standard and for the aqueous suspension of final insoluble residue of DCN from the control, gadoterate, and gadodiamide treated groups.

Gd in the insoluble fraction of DCN of animals treated with gadodiamide. Two Gd isotopes, ^{155}Gd and ^{158}Gd, were detected in these areas, proving unambiguously the presence of Gd. The NanoSIMS analysis also suggested the colocalization of Gd with calcium, phosphorus, oxygen, and, sometimes, with iron and sulfur. Some particles composed exclusively of iron were also detected. In addition, carbon and nitrogen were distributed in the whole analyzed region, which is consistent with the presence of organic matter, such as cell debris. However, these 2 elements were not specifically concentrated in the Gd-containing structures. The dimensions of 5 Gd-containing structures were estimated to be between 300–600 nm with the oxygen source and 350–500 nm with cesium source.

STEM With X-EDS Analysis

Figure 7 shows the STEM-EDX images of an agglomeration of various electron-dense particles detected in the insoluble fraction of DCN after gadodiamide treatment. The micrography (Fig. 7.1a) presents the entire agglomeration, and Figure 7.2a–4a shows 3 zones of interest obtained at higher magnifications, with the corresponding elemental

maps of Gd (Fig. 7b), Ca (Fig. 7c), P (Fig. 7d), Fe (Fig. 7e), and S (Fig. 7f).

A cluster composed of multiple spheroid particles (Fig. 7a, yellow vertical arrow) and separate spheroid particles (yellow horizontal arrow) rich in Gd was detected within the agglomeration (Fig. 7.1b). These electron dense structures of 100 to 150 nm for isolated particles reach around 1 μm for agglomerated ones (Fig. 7.1a) and show a very characteristic filamentous, spherulitic morphology (3a and 4a).

Some elements such Gd, Ca, and P are colocalized, which indicates that these structures are mainly composed of these 3 elements. Ca is rather homogenously distributed, although Gd and P are more concentrated in the core of the structure. Occasional or no colocalization of Gd with iron or with sulfur was observed. In addition, the distributions of C, N (cf. Fig. 3 in SDC, http://links.lww.com/RLI/A663), and S were homogenous, without any concentrated regions. This is consistent with the presence of cell debris in the insoluble DCN fraction and in favor of an inorganic composition for Gd structure detected in this magnified area.

Figure 8 presents a high-resolution TEM image of one of these spheroid structures showing that nanometric, electron-dense Gd particles are concentrated in its core. The electron diffraction analysis revealed the amorphous nature of the spheroid structure (diffusion pattern typical of amorphous structure).

DISCUSSION

Total Gd Concentrations

To address the speciation of the residual Gd in DCN, this study was carried out on rats injected with a cumulated dose of 50 mmol/kg after a 4-month wash-out period. This dose corresponds to 80-fold the usual clinical dose if adjusted for man and was chosen as a compromise between the long wash-out period and the minimum Gd concentration required to provide a full picture of the Gd speciation using multiple bioanalytical and imaging techniques.

The Gd concentrations measured in this study cannot be compared with most of the previously published data because they were not determined in the entire brain structure, such as cerebellum, but exclusively in the isolated DCN. Therefore, the Gd concentrations determined here are not affected by the dilution with the adjacent tissues. To our knowledge, only 2 previous studies focused on the rat DCN after repeated gadodiamide injections; the cumulative dose was 12 mmol/kg and the Gd concentration values were 27.1 ± 6.5 nmol/g (4.5-week wash-out period)[28] and 30 to 40 nmol/g (1-year wash-out period).[17] The differences between Gd concentrations found in the above 2 studies are most likely due to the use of different analytical methods and different preclinical designs. Indeed, the Gd concentration of 27.1 ± 6.5 nmol/g was determined in DCN of renally sensitized rats by ICP-MS. The other work was conducted in healthy rats using semiquantitative LA-ICP-MS. In our study, the Gd concentration determined in the pooled DCN using ICP-MS was 24.3 nmol/g for gadodiamide, which is comparable, in terms of concentration range, with the previous 2 studies.

Note that the Gd concentration after gadodiamide treatment was approximately 100 times higher than after macrocyclic gadoterate administration (0.25 nmol/g). This immense difference in the amount of residual Gd present after treatment with linear and M-GBCAs is consistent with the class effects already reported.[13]

To explore the Gd speciation, the DCN were progressively solubilized using the sequential extraction procedure that preserved the stability of intact GBCAs form, and the total Gd content in all resulting fractions was determined (Fig. 2). First, the sample was extracted with 100 mM ammonium acetate (pH 7.4). In these conditions, water-soluble components are extracted, including intact GBCAs. Whereas 53% (0.83 ng) of Gd from DCN of animals treated with gadoterate meglumine were recovered in that step, only 2% of total residual Gd (3.10 ng) were extracted from DCN of animals treated with gadodiamide.
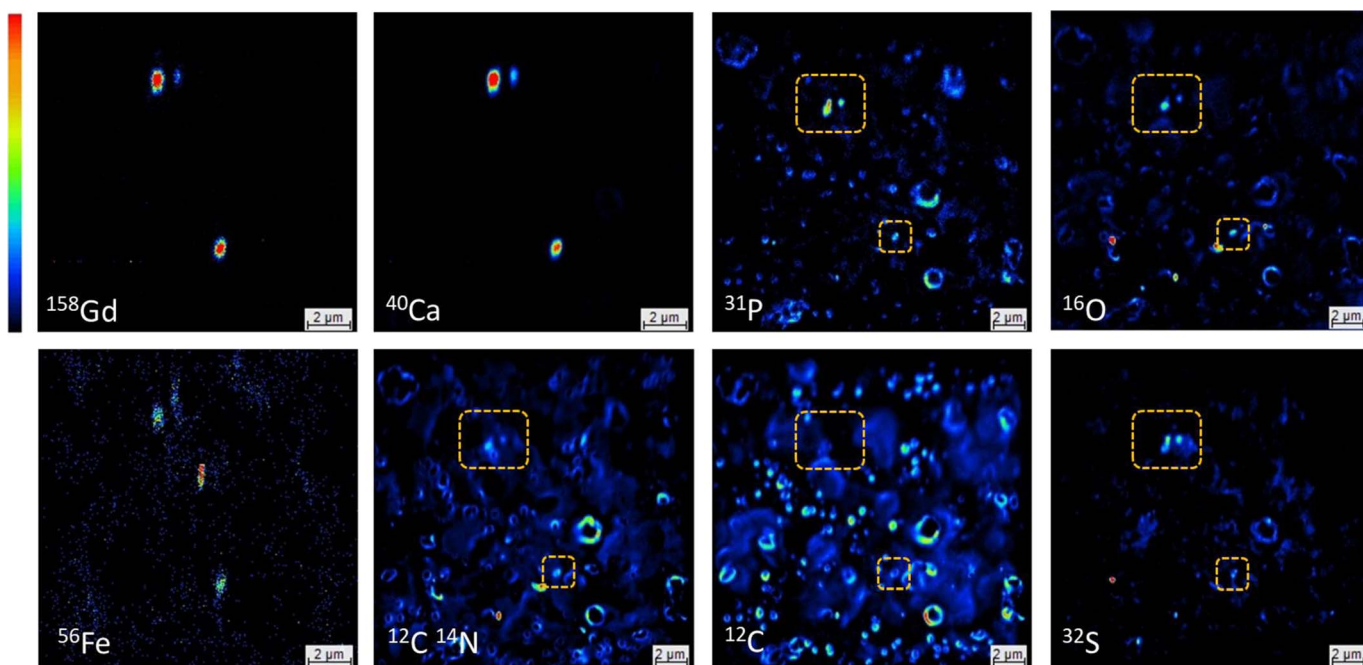
FIGURE 6. NanoSIMS mapping of 1 region of interest in the aqueous suspension of the final insoluble residue of pooled DCN from gadodiamide treated group, showing the ^{158}Gd, ^{40}Ca, ^{31}P, ^{16}O, ^{56}Fe, ^{12}C^{14}N, ^{12}C, and ^{32}S signals. The relative intensity of the signal is represented by a common color scale in the top left. Orange squares are used to indicate the position of the Gd-rich structures in the images of other elements.

In the subsequent extraction, the water-insoluble residue was solubilized using 5.6 M urea, which is a chaotropic agent commonly used to break the noncovalent interactions and consequently allowing one to solubilize more hydrophobic, membrane-associated proteins and proteoglycans.[29]

For gadoterate, the amount of Gd extracted in the 5.6 M urea-soluble was less than LLOQ$_{5.6M\ urea}$. For gadodiamide, although, initially, 11.8 ng of Gd was recovered, the dilution of this fraction decreased 4 times the amount of soluble Gd analyzed using SEC-ICP-MS. This behavior might suggest that part of species was only soluble in high concentration of urea.

Speciation of Soluble Gd Using SEC-ICP-MS

In the case of gadoterate, water-soluble Gd was present exclusively as 1 species eluting at the retention time of GBCA, which was demonstrated by Gianolio et al.[25] using a different chromatographic method (hydrophilic interaction chromatography–electrospray ionization mass spectrometry) and for another M-GBCA (gadoteridol) to be the intact GBCA form. For gadodiamide, apart from the tiny amount of Gd detected as the low-molecular-weight compounds (intact GBCA), a stable Gd-macromolecule complex of 440 kDa and likely labile complexes of Gd^{3+} with endogenous biomolecules were the dominating species (cf. Fig. 4). The presence of high-molecular-weight Gd forms in the cerebellum of animals treated with L-GBCAs was already reported in the literature; however, the identity of these macromolecules has not been established so far.[23,24] In our work, the retention time of Gd-containing macromolecules corresponded to that of ferritin. In addition, ^{54}Fe was eluted exactly at the same retention time as ^{158}Gd, which suggests the presence of an iron-containing macromolecule, such as ferritin. Because of the low resolution of SEC, the evidence of the identity of the ligand complexing iron and Gd is not formal. However, our observation is consistent with a previously reported study showing the binding of nanomolar concentrations of free Gd^{3+} ions released from GBCAs to the iron oxyhydroxide core of ferritin after 24 hours of incu-

bation at 37°C under similar physiological conditions (50 mM HEPES, pH 7.4, 0.9% NaCl).[30]

The morphology of the obtained chromatograms is consistent with that of those reported by Robert et al.[24] In this study, 5 months after injection, the major water-soluble Gd species detected in the cerebellum of rats injected with gadodiamide was not the intact GBCA but Gd bound to 2 classes of macromolecules (>66 kDa). Likewise, in our study, we observed a significantly lower intensity of the intact GBCA peak of gadodiamide compared with gadoterate. This strongly suggests that the residual Gd is no longer under its intact GBCA form and supports the hypothesis of Gd dechelation from L-GBCAs. Moreover, the column recoveries obtained for water-soluble Gd species showed a substantial difference between macrocyclic gadoterate and linear gadodiamide. Whereas for gadoterate 95% of water-soluble Gd was eluted from the chromatographic column, only 32% was eluted for gadodiamide. Even though SEC is considered to be one of the mildest chromatographic separation modes, it is associated with an incomplete recovery of ionic forms of metals or weak metal complexes.[31] Therefore, our results suggest that, for gadodiamide, a significant amount of Gd was present in the form of dissociated Gd^{3+} weakly bound to some endogenous molecules of so far unknown nature. Consequently, these complexes were not stable in the chromatographic conditions, resulting in retention of Gd^{3+} on the stationary phase and invisible (to ICP-MS) elution of the corresponding ligand.

For gadodiamide, the second step of the extraction allowed the recovery of not only the intact GBCA form and macromolecular 440 kDa but also of a high-molecular-weight species with a molecular weight estimated to exceed 660 kDa. It should be highlighted that this species was absent in the water-soluble fraction and was eluted very close to the void volume of the chromatographic column, strongly suggesting the presence of very large molecules such as proteoglycans or aggregates.

In 2 animal studies, it was shown that the increased signal intensity in the DCN of rats persisted for at least 1 year after administration of L-GBCAs.[24,32] It was discussed previously that because of the high relaxivities, the species that could produce this enhancement are intact
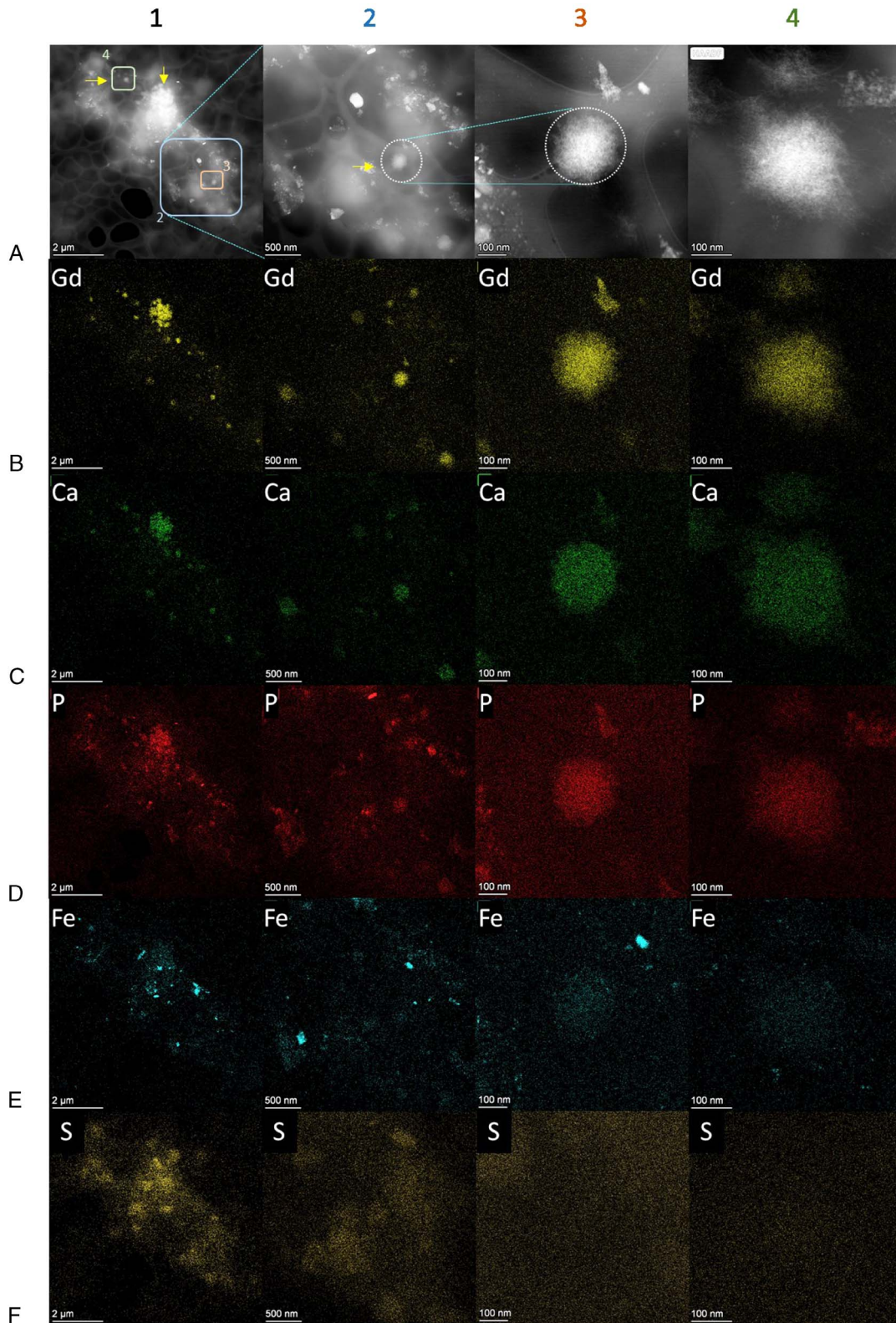
FIGURE 7. A, STEM/X-EDS images of aqueous suspension (dry) of insoluble fraction of DCN of rats treated with gadodiamide. Column 1 images show typical agglomeration of multiple particles present in the insoluble fraction; columns 2 and 3 correspond to column 1 at higher magnifications, whereas column 4 presents details of an isolated particle. B–F correspond to elemental cartographies (B for Gd, C for Ca, D for P, E for Fe, and F for S element) obtained using X/EDS for the selected ROI.
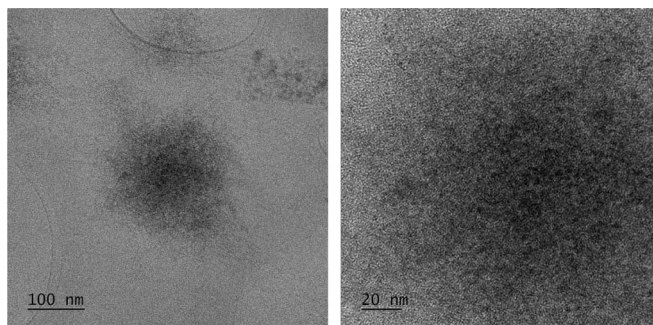
FIGURE 8. TEM images of aqueous suspension of insoluble fraction of DCN from the animals treated with gadodiamide. A, Sea urchin–like Gd deposit; B, high-resolution image.

GBCA and Gd bound to macromolecules. In our work, the low-molecular-weight compounds, such as intact gadodiamide, represented approximately 5% of the soluble Gd species, which might be insufficient to account for the signal enhancement on the T1-weighted MR images. Thus, the complementary contribution to the signal enhancement most likely came from Gd bound to macromolecules that account for approximately 24% of soluble Gd species. However, the soluble species account for less than 10% of total Gd present in DCN; therefore, further studies are necessary to evaluate whether this amount of Gd could be responsible for the magnitude of the enhancement observed in DCN.

Insight Into Insoluble Gd by SP-ICP-MS

The sequential extraction procedure allowed for a significantly better solubilization of DCN as well as for the reduction of potential interferences in the final insoluble residue. Despite its simplification, for linear gadodiamide, it contained the major portion of Gd, which accounts for 110 ng of the element.

The determination of the nature of Gd species in the insoluble fraction can be addressed using SP-ICP-MS, which is becoming an important tool for the characterization of metallic nanoparticles.[33] Indeed, the SP-ICP-MS can discriminate whether Gd is present in the sample in its soluble form (Gd^{3+}) or in an insoluble form. For the purpose of SP-ICP-MS, the Gd species were preconcentrated using water and urea extractions into the final insoluble residue, which was further resuspended in water. Figure 5 shows the ^{158}Gd time scan obtained for an ionic Gd^{3+} standard with its typical continuous signal, whereas for the insoluble fraction of DCN of rats treated with gadodiamide a significant number of signal spikes was observed. The latter confirms that Gd was present in its particulate form in the insoluble part of DCN of animals treated with gadodiamide. In the case of gadoterate, the time scan was similar to that of the control.

Characterization of Insoluble Gd Species Using NanoSIMS and STEM-EDX

Nanoscale secondary ion mass spectrometry and STEM-EDX allowed the detection of Gd species in trace amount in the insoluble fraction of the DCN. Nanoscale secondary ion mass spectrometry imaging revealed the presence of ellipsoid Gd-containing structures with average size between 350 and 500 nm that were associated with calcium, oxygen, phosphorus, and sometimes with iron and sulfur.

For further characterization of the detected insoluble Gd species and their colocalization with endogenous elements, STEM-EDX was used. Indeed, elemental mapping with higher lateral resolution (1 nm) compared with NanoSIMS (100 nm) was obtained using STEM-EDX. Likewise, a Gd map of analyzed agglomeration was acquired and allowed the differentiation of characteristic spheroid structures of 100 to 150 nm from other electron-dense particles. Similarly to NanoSIMS analysis, these spheroid, amorphous Gd species were mainly composed of calcium and phosphorus. However, no colocalization with either iron or sulfur was observed. This discrepancy may be attributed to the slightly lower

spatial resolution of NanoSIMS in comparison with STEM or to the different sensitivities of these techniques.

The evidence emerging from these data is that residual Gd present in the insoluble DCN fraction is in the particulate form, composed mainly of mixed Gd/Ca phosphate salts. Indeed, our results are in good agreement with the previous studies of human skin samples from patients suffering from systemic nephrogenic fibrosis showing the association of insoluble Gd deposits with Ca, P, and only sometimes with Fe.[34,35] Furthermore, our data are also consistent with the findings reported in the recent study demonstrating the occurrence of very similar spheroid Gd-rich structures referred to as "sea urchin-like" in DCN of rat with moderately impaired renal function after administration of L-GBCAs: gadobenate and gadodiamide.[22] Similarly to our STEM/X-EDS results, iron was not detected in these Gd-rich insoluble structures.

The determination of Gd concentration in the insoluble fraction demonstrated that the detected species account for 70% of Gd retained in DCN. Single-particle ICP-MS confirmed that they were present mainly in particulate form. Therefore, the sea urchin-like structure is very likely the dominant Gd species in DCN, and its contribution to T1 signal enhancement on MR images could be relevant. Indeed, because of the relatively complex, sea urchin-like morphology, the access of Gd to water molecules in this porous structure cannot be excluded. Furthermore, the characteristics of these amorphous deposits remain unknown; thus, it is difficult to evaluate whether Gd could be potentially released from it. Even if the contribution of mixed Gd/Ca phosphate salts to the signal enhancement is uncertain, it is responsible for prolonged or permanent deposition of Gd in the DCN and very likely also in other brain structures.

The Gd speciation data emerging from this study contribute to the understanding of the fate of GBCAs in vivo. Indeed, Rasschaert[36] suggested that Gd can reach the brain as the intact GBCA form through the choroid plexus situated in the ventricles. Part of GBCAs would cross the ependymal cells of ventricles and diffuse to interstitium. In the case of L-GBCAs, once they access the structures rich in metals, their transmetallation would induce the formation of new Gd species. Indeed, in our study, the major fraction of Gd retained in DCN 4 months after gadodiamide administration was found not in the intact GBCA form. Most likely, it was present as dechelated Gd^{3+} in the insoluble mixed metal phosphate salts, soluble macromolecules suggested to be ferritin, and as labile complexes with endogenous ligands. Therefore, the preferential accumulation of Gd in the specific structures such as DCN would not be triggered by Gd affinity toward a specific target in the tissue itself but would be a consequence of the high metal content of this structure in comparison with adjacent brain structures. However, alternative hypotheses were also put forward.[37] Because the available data regarding the amorphous Gd/Ca phosphate salts in the human body are limited,[38] further studies are needed to evaluate the biological impact of its presence in the brain.

The main limitation of our study is the lack of analytical replicates. Indeed, because of the very small mass of rat DCN and for ethical reasons, DCN from 6 animals needed to be pooled and were treated as 1

sample. The second limitation is related to the sample preparation procedure before the analyses. The tissue homogenization disrupts cell membranes and exposes extracellular GBCAs and other Gd species to the intracellular components which can affect the equilibria present in vivo. Although the stability of GBCAs in the conditions of the sequential extraction procedure was previously verified,[26] the integrity of other, more fragile Gd species could be altered.

CONCLUSION

Hyphenated techniques combined with high-resolution imaging allowed, for the first time, a comprehensive Gd speciation analysis in DCN of rats repeatedly injected with gadoterate meglumine or gadodiamide. Four months after the injections, the major amount of Gd was present as intact GBCA. In contrast, after administration of linear gadodiamide, the soluble DCN fractions were composed mainly of high-molecular-weight Gd species of approximately 440 kDa. One of them was speculated to be a Gd complex with iron-binding protein (ferritin). However, the major amount (70%) of residual Gd was found in the insoluble fraction of DCN in a particulate form, very likely composed of mixed Gd/Ca phosphates. The evidence emerging from this study corroborates the in vivo dechelation hypothesis of L-GBCAs and highlights the high potential of cutting-edge techniques and the need for complementary analytical approaches to better understand the mechanisms of the Gd deposition in the brain.

REFERENCES

1. Kanda T, Ishii K, Kawaguchi H, et al. High signal intensity in the dentate nucleus and globus pallidus on unenhanced T1-weighted MR images: relationship with increasing cumulative dose of a gadolinium-based contrast material. *Radiology.* 2014;270:834–841.
2. Runge VM. Safety of the gadolinium-based contrast agents for magnetic resonance imaging, focusing in part on their accumulation in the brain and especially the dentate nucleus. *Invest Radiol.* 2016;51:273–279.
3. Kanda T, Fukusato T, Matsuda M, et al. Gadolinium-based contrast agent accumulates in the brain even in subjects without severe renal dysfunction: evaluation of autopsy brain specimens with inductively coupled plasma mass spectroscopy. *Radiology.* 2015;276:228–232.
4. McDonald RJ, McDonald JS, Kallmes DF, et al. Intracranial gadolinium deposition after contrast-enhanced MR imaging. *Radiology.* 2015;275:772–782.
5. Grobner T. Gadolinium—a specific trigger for the development of nephrogenic fibrosing dermopathy and nephrogenic systemic fibrosis? *Nephrol Dial Transplant.* 2006;21:1104–1108.
6. Sieber MA, Pietsch H, Walter J, et al. A preclinical study to investigate the development of nephrogenic systemic fibrosis: a possible role for gadolinium-based contrast media. *Invest Radiol.* 2008;43:65–75.
7. Idée J-M, Fretellier N, Robic C, et al. The role of gadolinium chelates in the mechanism of nephrogenic systemic fibrosis: a critical update. *Crit Rev Toxicol.* 2014;44:895–913.
8. European Medicines Agency. EMA's final opinion confirms restrictions on use of linear gadolinium agents in body scans. http://www.ema.europa.eu/docs/en_gb/document_library/referrals_document/gadolinium_contrast_agents_31/european_commission_final_decision/wc500240575.pdf. Accessed October 8, 2020.
9. Food and Drug Administration. FDA drug safety communication: FDA warns that gadolinium-based contrast agents (GBCAs) are retained in the body; requires new class warnings. https://www.fda.gov/drugs/drugsafety/ucm589213.htm. Accessed October 10, 2020.
10. Lancelot E, Desché P. Gadolinium retention as a safety signal: experience of a manufacturer. *Invest Radiol.* 2020;55:20–24.
11. Robert P, Lehericy S, Grand S, et al. T1-weighted hypersignal in the deep cerebellar nuclei after repeated administrations of gadolinium-based contrast agents in healthy rats: difference between linear and macrocyclic agents. *Invest Radiol.* 2015;50:473–480.
12. Robert P, Violas X, Grand S, et al. Linear gadolinium-based contrast agents are associated with brain gadolinium retention in healthy rats. *Invest Radiol.* 2016;51:73–82.
13. Robert P, Frenzel T, Factor C, et al. Methodological aspects for preclinical evaluation of gadolinium presence in brain tissue: critical appraisal and suggestions for harmonization—a joint initiative. *Invest Radiol.* 2018;53:499–517.
14. Port M, Idée J-M, Medina C, et al. Efficiency, thermodynamic and kinetic stability of marketed gadolinium chelates and their possible clinical consequences: a critical review. *Biometals.* 2008;21:469–490.
15. Frenzel T, Lengsfeld P, Schirmer H, et al. Stability of gadolinium-based magnetic resonance imaging contrast agents in human serum at 37 degrees C. *Invest Radiol.* 2008;43:817–828.
16. Hallgren B, Sourander P. The effect of age on the non-haemin iron in the human brain. *J Neurochem.* 1958;3:41–51.
17. El Hamrani D, Vives V, Buchholz R, et al. Effect of long-term retention of gadolinium on metabolism of deep cerebellar nuclei after repeated injections of gadodiamide in rats. *Invest Radiol.* 2020;55:120–128.
18. Gianolio E, Gregorio ED, Aime S. Chemical insights into the issues of Gd retention in the brain and other tissues upon the administration of Gd-containing MRI contrast agents. *Eur J Inorg Chem.* 2019;2019:137–151.
19. Tweedle MF. Gadolinium deposition: is it chelated or dissociated gadolinium? How can we tell? *Magn Reson Imaging.* 2016;34:1377–1382.
20. Le Fur M, Caravan P. The biological fate of gadolinium-based MRI contrast agents: a call to action for bioinorganic chemists. *Metallomics.* 2019;11:240–254.
21. Davies J, Marino M, Smith APL, et al. Repeat and single dose administration of gadodiamide to rats to investigate concentration and location of gadolinium and the cell ultrastructure. *Sci Rep.* 2021;11:13950.
22. Rasschaert M, Schroeder JA, Wu T-D, et al. Multimodal imaging study of gadolinium presence in rat cerebellum: differences between Gd chelates, presence in the Virchow-Robin space, association with lipofuscin, and hypotheses about distribution pathway. *Invest Radiol.* 2018;53:518–528.
23. Frenzel T, Apte C, Jost G, et al. Quantification and assessment of the chemical form of residual gadolinium in the brain after repeated administration of gadolinium-based contrast agents: comparative study in rats. *Invest Radiol.* 2017;52:396–404.
24. Robert P, Fingerhut S, Factor C, et al. One-year retention of gadolinium in the brain: comparison of gadodiamide and gadoterate meglumine in a rodent model. *Radiology.* 2018;288:424–433.
25. Gianolio E, Bardini P, Arena F, et al. Gadolinium retention in the rat brain: assessment of the amounts of insoluble gadolinium-containing species and intact gadolinium complexes after repeated administration of gadolinium-based contrast agents. *Radiology.* 2017;285:839–849.
26. Strzeminska I, Factor C, Robert P, et al. Speciation analysis of gadolinium in the water-insoluble rat brain fraction after administration of gadolinium-based contrast agents. *Invest Radiol.* 2021;56:535–544.
27. Malherbe J, Penen F, Isaure M-P, et al. A new radio frequency plasma oxygen primary ion source on nano secondary ion mass spectrometry for improved lateral resolution and detection of electropositive elements at single cell level. *Anal Chem.* 2016;88:7130–7136.
28. Rasschaert M, Emerit A, Fretellier N, et al. Gadolinium retention, brain T1 hyperintensity, and endogenous metals: a comparative study of macrocyclic versus linear gadolinium chelates in renally sensitized rats. *Invest Radiol.* 2018;53:328–337.
29. Karamanos NK, Aletras AJ, Antonopoulos CA, et al. Extraction and fractionation of proteoglycans from squid skin. *Biochim Biophys Acta.* 1988;966:36–43.
30. Neburkova J, Rulseh AM, Chang SLY, et al. Formation of gadolinium–ferritin from clinical magnetic resonance contrast agents. *Nanoscale Adv.* 2020;2:5567–5571. doi:10.1039.C9NA00567F.
31. Schaumlöffel D, Ouerdane L, Bouyssiere B, et al. Speciation analysis of nickel in the latex of a hyperaccumulating tree *Sebertia acuminata* by HPLC and CZE with ICP MS and electrospray MS-MS detection. *J Anal At Spectrom.* 2003;18:120–127.
32. Jost G, Frenzel T, Boyken J, et al. Long-term excretion of gadolinium-based contrast agents: linear versus macrocyclic agents in an experimental rat model. *Radiology.* 2019;290:340–348.
33. Mozhayeva D, Engelhard C. A critical review of single particle inductively coupled plasma mass spectrometry—a step towards an ideal method for nanomaterial characterization. *J Anal At Spectrom.* 2020;35:1740–1783.
34. Thakral C, Abraham JL. Gadolinium-induced nephrogenic systemic fibrosis is associated with insoluble Gd deposits in tissues: in vivo transmetallation confirmed by microanalysis. *J Cutan Pathol.* 2009;36:1244–1254.
35. Abraham JL, Chandra S, Thakral C, et al. SIMS imaging of gadolinium isotopes in tissue from nephrogenic systemic fibrosis patients: release of free Gd from magnetic resonance imaging (MRI) contrast agents. *Appl Surf Sci.* 2008;255:1181–1184.
36. Rasschaert M. Capture cérébrale de chélates de gadolinium: imagerie multimodale et analyse des conséquences neurotoxicologiques [Brain Uptake of Gadolinium Chelates: Multimodal Imaging and Analysis of Neurotoxicological Consequences] [dissertation]. Gif-sur-Yvette, France: Universite Paris-Saclay;2019.
37. Rasschaert M, Weller RO, Schroeder JA, et al. Retention of gadolinium in brain parenchyma: pathways for speciation, access, and distribution. A critical review. *J Magn Reson Imaging.* 2020;52:1293–1305.
38. Gelli R, Ridi F, Baglioni P. The importance of being amorphous: calcium and magnesium phosphates in the human body. *Adv Colloid Interface Sci.* 2019;269:219–235.